Layer-by-layer assembled multilayers using catalase-encapsulated gold nanoparticles

2010 Nanotechnology 21 375702

(http://iopscience.iop.org/0957-4484/21/37/375702)

Nanotechnology **21** (2010) 375702 (8pp) doi:10.1088/0957-4484/21/37/375702

Layer-by-layer assembled multilayers using catalase-encapsulated gold nanoparticles

Sungwoo Kim[1,3], **Jeongju Park**[1,3] **and Jinhan Cho**[2]

[1] School of Advanced Materials Engineering, Kookmin University, Jeongneung-dong, Seongbuk-gu, Seoul 136-702, Korea
[2] Department of Chemical and Biological Engineering, Korea University, Anam-dong, Seongbuk-gu, Seoul 136-701, Korea

E-mail: jinhan71@korea.ac.kr

Received 16 January 2010, in final form 14 June 2010
Published 20 August 2010
Online at stacks.iop.org/Nano/21/375702

Abstract
We introduce a novel and versatile approach for the preparation of multilayers, based on catalase-encapsulated gold nanoparticles (CAT-Au_{NP}), allowing electrostatic charge reversal and structural transformation through pH adjustment. CAT-Au_{NP}, which are synthesized directly from CAT stabilizer, can be electrostatically assembled with anionic and cationic PEs as a result of the charge reversal of the catalase stabilizers through pH control. In particular, at pH 5.2, near the *pI* of catalase, dispersed CAT-Au_{NP} are structurally transformed into colloidal or network CAT-Au_{NP} nanocomposites. Furthermore, we demonstrate that the layer-by-layer assembled multilayers composed of PEs and CAT-Au_{NP} induce an effective electron transfer between CAT and the electrode as well as a high loading of CAT and Au_{NP}, and resultantly exhibit a highly catalytic activity toward H_2O_2.

S Online supplementary data available from stacks.iop.org/Nano/21/375702/mmedia

(Some figures in this article are in colour only in the electronic version)

1. Introduction

Biocatalytic proteins have been extensively used in a variety of applications such as biological and electrochemical sensing devices because they can be activated and regenerated by the exchange of electrons between the electrodes and proteins [1–12]. Generally, with redox proteins in the solution state it is usually difficult to exchange electrons directly with bare electrodes, and resultantly many efforts have been devoted to incorporating the proteins into ultrathin films modified on the electrode surface. Such films can provide a suitable electrochemical environment for redox proteins and facilitate the electron exchange between the proteins and underlying electrodes. Another remarkable approach for redox protein films is that metal nanoparticles are incorporated into proteins. For example, the direct electrochemical behavior of various proteins such as horseradish peroxidase, microperoxidase, myoglobin or catalase (CAT) has been observed by the well-behaved cyclic voltammetry (CV) responses for protein-based films on gold nanoparticle (Au_{NP}) or platinum nanoparticle (Pt_{NP})-coated electrodes [13–17]. Recently, Au_{NP} functionalized with the flavin adenine dinucleotide and pyrroloquinoline quinine cofactors were employed respectively for the reconstitution of apo-glucose oxidase and apo-glucose dehydrogenase enzymes on the electrode surface [6, 14]. In this case, the enhancement of the direct electron transfer of redox enzymes was achieved by nanosized Au_{NP}.

There are various methods to prepare protein films, among which the layer-by-layer (LbL) assembly method offers diverse opportunities to prepare hybrid nanocomposite films with tailored functional properties and multilayer structure. An important advantage of this method is that it enables the preparation of films with controlled thickness, composition and functionality on substrates of different size and shape [1–3, 18–27]. The basic principle of LbL assembly is originally from the alternate adsorption of oppositely charged polyelectrolytes (PEs) on solid surfaces using

[3] Two authors are equally contributed to this work.

complementary interactions (i.e., electrostatic, hydrogen-bonding or covalent interaction), and recently extended to fabricate multilayered protein films. Particularly, since metal nanoparticles have unique properties, they are also used to assemble LbL multilayers with redox proteins. The redox proteins in multilayer films with nanoparticles exhibit direct and reversible cyclic voltammetry (CV) responses at the underlying electrodes. For example, it was reported that myoglobin/Au_{NP} multilayers showed higher surface concentrations of electroactive proteins and better electrocatalytic activity, mainly because of the high conductivity of the Au_{NP}, which may efficiently tunnel electrons between the proteins and the electrodes [22]. To date, protein multilayers containing metal nanoparticles have been prepared from alternate adsorption between proteins and nanoparticles. However, to the best of our knowledge, electrostatic LbL assembly using protein-encapsulated Au_{NP} and their electrochemical study has not yet been reported.

In this work, we introduce a novel strategy for the preparation of protein-encapsulated metal nanoparticles and their nanocomposite multilayers. The strategy is based on the use of protein-encapsulated Au_{NP} synthesized directly from protein stabilizer. We highlight the fact that these hybrid nanoparticles allow electrostatic charge reversal through pH control, high loading of proteins through structural transformation (from well-dispersed nanoparticles to network structures according to the solution pH), efficient electron transfer between proteins and electrode, porous structures and resultantly exhibit a higher electrochemical activity than those based on conventional multilayered sensors such as PE/protein or protein/Au_{NP} multilayers. Therefore, we believe that our approach can be used to exert a wide range of control over the preparation of various protein–metal-based multilayers with highly biocatalytic activity and a high loading of functional components.

2. Experimental sections

2.1. Materials

Anionic poly(sodium 4-styrene sulfonate) (PSS) (M_w = 70 000), cationic poly(allylamine hydrochloride) (PAH) (M_w = 70 000) and catalase were purchased from Aldrich. Catalase-stabilized Au nanoparticles (CAT-Au_{NP}) were synthesized as follows: 50 ml of 0.45 or 1.75 mM $HAuCl_4$ was maintained at room temperature while stirring vigorously. The initial solution pH was adjusted to 9. In this case, rapid addition of 50 ml of 2 mg ml^{-1} catalase to the vortex of the solution and successive addition (1 ml) of 70 mM $NaBH_4$ resulted in a color change from pale yellow to red. After injection of $NaBH_4$ into the CAT-$AuCl_4^-$ solution, the pH of the CAT-Au_{NP} solution was increased from pH 9.0 to 9.7. The resultant CAT-Au_{NP} solution was adjusted to pH 9 by further addition of 0.1 M HCl. The diameter size of the CAT-Au_{NP} was measured to be about 9 ± 3.5 nm (50 particles sampled) as confirmed by TEM images. The direct synthesis of gold nanoparticles from enzyme stabilizer implies the fact that amine and carboxylic acid groups, $–NH_2$ and –COOH [28, 29] of enzyme stabilizers could be used as effective stabilizers during the synthesis of the Au_{NP}.

Anionic citrate-stabilized Au nanoparticles (citrate-Au_{NP}) were synthesized by the citrate reduction method. Briefly, 185 mg $HAuCl_4$ was dissolved in an aqueous solution of 220 ml containing 400 mg of the citrate ion stabilizer. Rapid addition of 1 ml of 70 mM sodium citrate to the vortex of the solution resulted in a color change from pale yellow to deep purple. The diameter of the synthesized Au_{NP} was about 12 ± 3 nm (100 particles sampled).

2.2. Preparation of LbL multilayer films

The solution pH of CAT-Au_{NP} prepared from pH 9 CAT-$AuCl_4^-$ solution increased to about 9.7 as a result of the addition of the $NaBH_4$ reducing agent. The CAT-Au_{NP} solution was readjusted to pH 9 by addition of 0.1 M HCl. For the build-up of PAH/dispersed CAT-Au_{NP} multilayers, the pH of both the PAH (1 mg ml^{-1}) and CAT-Au_{NP} solutions (2 mg ml^{-1}) was first adjusted to pH 9 by addition of 0.1 M HCl. The Si substrates had an anionic surface by heating at 65 °C for 5 s in a 5:1:1 vol% mixture of water, hydrogen peroxide, and 29% ammonia solution (RCA solution). These substrates were first dipped for 10 min in the cationic PAH solution (pH 9), washed twice by dipping in pH 9 water for 1 min, and air-dried with a gentle stream of nitrogen. Anionic CAT-Au_{NP} (pH 9) was subsequently deposited onto the PAH-coated substrates by using the same adsorption, washing, and drying procedures as described above. This process was repeated until the desired number of layers was deposited.

For preparing (PAH/CAT-Au_{NP} colloids)$_n$ multilayers, the solution pH of the dispersed CAT-Au_{NP} was first adjusted to pH 5.2 near the *pI* of CAT. In this case, positively charged CAT-Au_{NP} colloids were formed, and then the consecutive LbL deposition of PSS/PAH/PSS (0.1 M NaCl was added to pH 5.2 PAH and PSS solutions) was performed onto the CAT-Au_{NP} composite colloids. After these processes, the pH of the PSS/PAH/PSS-encapsulated CAT-Au_{NP} colloidal solution was adjusted to pH 9 using 0.1 M NaOH. The LbL deposition process for the preparation of (PAH/CAT-Au_{NP} colloids)$_n$ multilayers onto the planar substrates was identical to that of PAH/dispersed CAT-Au_{NP} multilayers.

2.3. Thickness measurements

The total thicknesses of (PE/CAT-Au_{NP})$_n$ multilayer films were measured from FE-SEM tilted images (i.e., the total thicknesses were compensated for the tilted angle of 12.5°).

2.4. Quartz crystal microgravimetry (QCM) measurements

A QCM device (model: QCM200, SRS) was used to investigate the mass of material deposited after each adsorption step. The resonance frequency of the QCM electrodes was ca. 5 MHz. The adsorbed mass of PEs and Au_{NP}, Δm, can be calculated from the change in QCM frequency, ΔF, according to the Sauerbrey equation [30]: ΔF (Hz) = $-56.6 \times \Delta m_A$, where Δm_A is the mass change per quartz crystal unit area, in μg cm^{-2}.

2.5. Thermogravimetric analysis

The aggregated CAT-Au_{NP} for dispersed and network CAT-Au_{NP} at pH 5.6 were first filtered and dried. Then, the powder was annealed by increasing the temperature to 700 °C at a heating rate of 5 °C min^{-1}. After a thermal treatment, the amount ratio of thermally decomposed CAT and Au_{NP} was obtained.

2.6. Cyclic voltammogram (CV) measurements

The electrochemical activity of multilayers adsorbed onto the QCM Au electrode was investigated by cyclic voltammograms (CVs) (model: compactstat, IVIUM). For sensing H_2O_2, the stock solutions of H_2O_2 were adjusted to a concentration of 21 mM at pH 7. It was reported that H_2O_2 can be generated by the following reaction:

$$\text{CatalaseFe}^{\text{III}} + H_2O_2 \longrightarrow [\text{CatalaseFe}^{\text{IV}}{=}O]^* + H_2O$$

$$[\text{CatalaseFe}^{\text{IV}}{=}O]^* + H_2O_2 \longrightarrow \text{CatalaseFe}^{\text{III}} + O_2 + H_2O.$$

2.7. Size of CAT-Au_{NP} and surface morphology of multilayers

The sizes of CAT-Au_{NP} synthesized at various solution pH were investigated by HR-TEM (model: JEM-3010, JEOL). The surface morphology of (PE/CAT-Au_{NP}) multilayers adsorbed onto Si substrates was measured with FE-SEM (model: JSM-7401F, JEOL).

2.8. Zeta-potential measurement

The zeta-potentials of catalase were measured using an electrophoretic light scattering spectrophotometer (ELS-8000) when the respective micelles were alternately adsorbed onto 600 nm diameter silica particles. (CAT-Au_{NP}/PSS)$_1$/CAT-Au_{NP}-coated silica particles were prepared as follows: 100 μl of a concentrated dispersion (6.4 wt%) of negatively charged 600 nm silica particles was diluted to 0.5 ml with deionized water. To this, 0.5 ml of CAT-Au_{NP} (1 mg ml^{-1} at pH 3) was added and, after 20 min, the excess catalase was removed by three repeated centrifugations (7000g, 5 min)/wash cycles. PSS (1 mg ml^{-1} at pH 3) with the addition of 0.5 M NaCl was then deposited onto the CAT-Au_{NP}-coated silica colloids using the same conditions. The above process was repeated until five layers were deposited and then zeta-potentials of these colloids were measured with increasing pH from 3 to 10 (see supporting information, figure S1 available at stacks.iop.org/Nano/21/375702/mmedia).

3. Results and discussion

The zeta-potential of CAT was measured as a function of pH. The measured *pI* (i.e., isoelectric point) was 5.6 [5, 6, 16]. Therefore, CAT has an overall positive charge at pH $<$ 5.6 and a negative charge at pH $>$ 5.6. This suggests that CAT-Au_{NP} can be assembled with anionic and cationic PEs

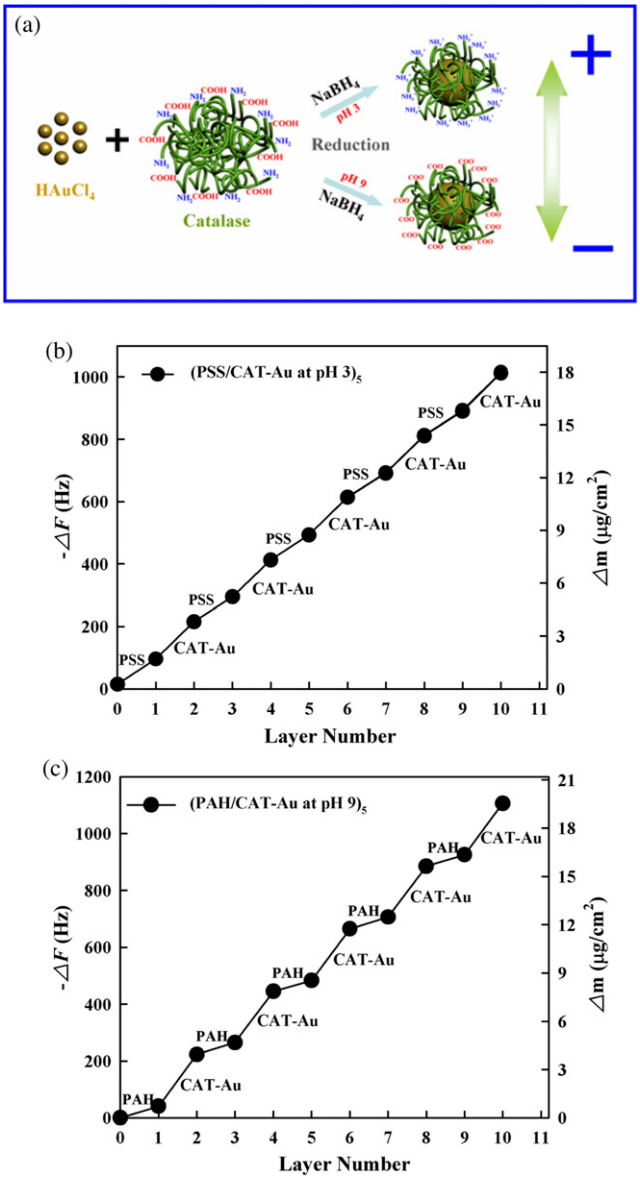

Figure 1. (a) Schematic for the synthesis of catalase-stabilized Au (CAT-Au_{NP}) nanoparticles with pH-dependent electrostatic properties. (b) TEM images, (c) UV–vis spectra and (d) the resultant size of CAT-Au_{NP} prepared at different initial solution pHs.

according to the solution pH of the CAT-Au_{NP} as schematically shown in figure 1(a). As confirmed from the quartz crystal microbalance (QCM) measurements, the LbL multilayer films were composed of anionic poly(styrene sulfonate) (PSS) and cationic CAT-Au_{NP}, which were assembled electrostatically at solution pH 3 after synthesizing the CAT-Au_{NP} at pH 9, and had a regular amount of PSS adsorbed (frequency change, $\Delta F \approx 82$ Hz and mass change, $\Delta m \approx 1$ μg cm^{-2}) and CAT-Au_{NP} ($\Delta F \approx 165$ Hz and $\Delta m \approx 2.0$ μg cm^{-2}) per layer with increasing deposition layer number (figure 1(b)). However, when the pH of the CAT-Au_{NP} solution was changed from 3 to 9, the CAT-Au_{NP} could be bonded electrostatically to cationic PAH due to charge reversal of the CAT stabilizers. Hence, these two oppositely charged layers could induce a build-up of multilayers (figure 1(c)). The adsorbed amount of

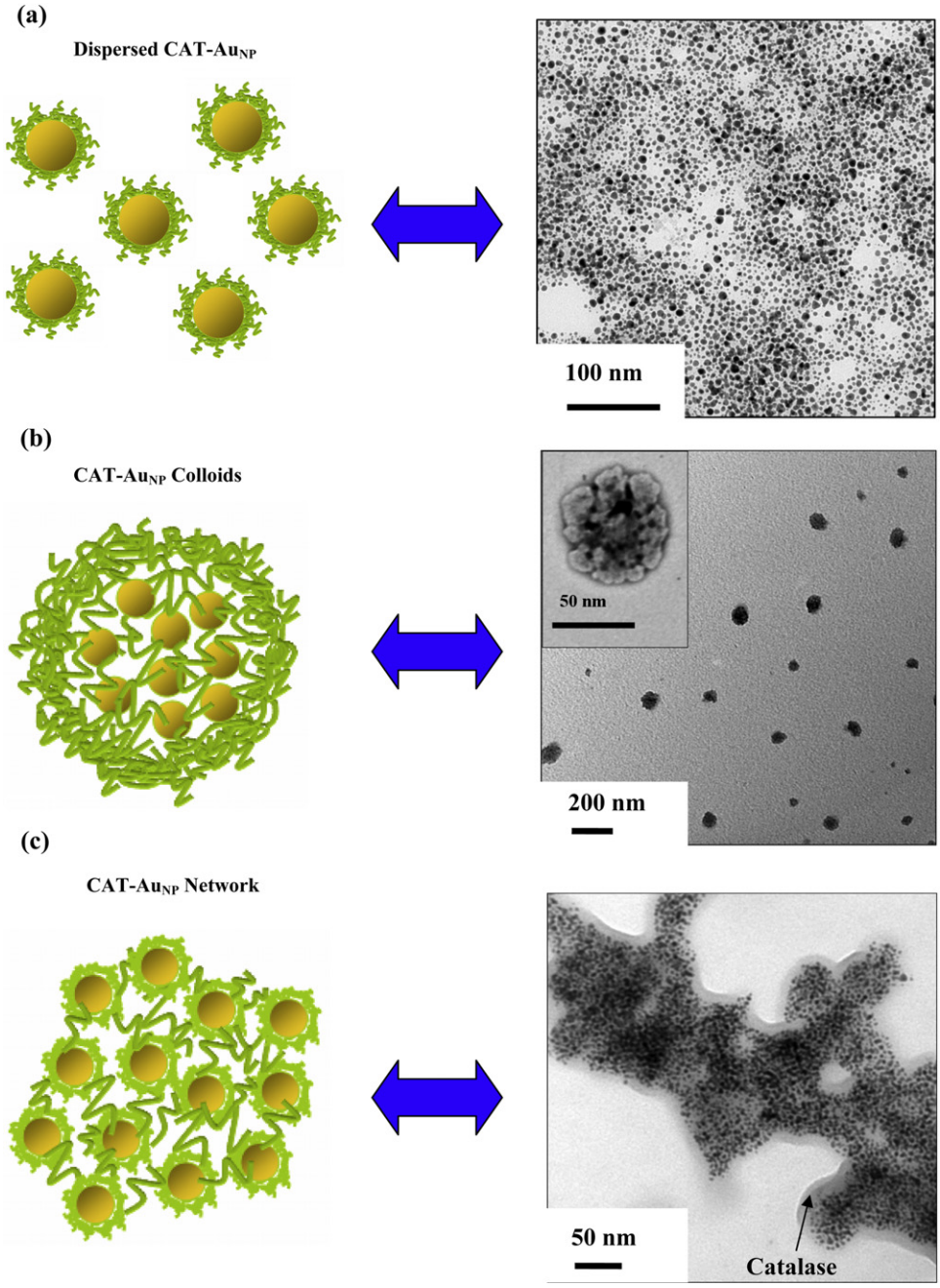

Figure 2. Schematic and TEM images for the preparation of CAT-Au$_{NP}$ with (a) dispersed, (b) colloidal and (c) network structures.

PAH and CAT-Au$_{NP}$ was measured to be approximately $\Delta m \approx 0.42\ \mu g\ cm^{-2}$ ($\Delta F \approx 35$ Hz) and $\Delta m \approx 2.54\ \mu g\ cm^{-2}$ ($\Delta F \approx 210$ Hz) per layer, respectively.

An additional benefit of the CAT-Au$_{NP}$ is that the pH-dependent electrostatic properties of CAT-Au$_{NP}$ can control the structure of the hybrid nanocomposite. In order to test this hypothesis, the solution pH of CAT-Au$_{NP}$ was adjusted to pH 5.2 near the *pI* of CAT. It should be noted that CAT-Au$_{NP}$ was well dispersed due to relatively strong electrostatic repulsion between the same charged nanoparticles at pH 9, as shown in figure 2. In this case, the well-dispersed CAT-Au$_{NP}$ was converted to agglomerated nanocomposite colloids with a diameter of 50 ± 20 nm at pH 5.2, presumably due to the formation of an electrostatic complex salt between the carboxylate ions and protonated amine functionality within the CAT stabilizers. In this case, it was observed that the surface plasmon absorbance peak of colloidal CAT-Au$_{NP}$ aggregates was significantly red-shifted from 550 (for dispersed CAT-Au$_{NP}$) to 577 nm (see supporting information, figure S2 available at stacks.iop.org/Nano/21/375702/mmedia).

Although the diameter of the catalase crystals without Au$_{NP}$ could be increased to 0.3–2 μm (see supporting information, figure S3 available from stacks.iop.org/Nano/21/375702/mmedia), the decrease in the free functional groups within the CAT-Au$_{NP}$ colloids as a result of the formation

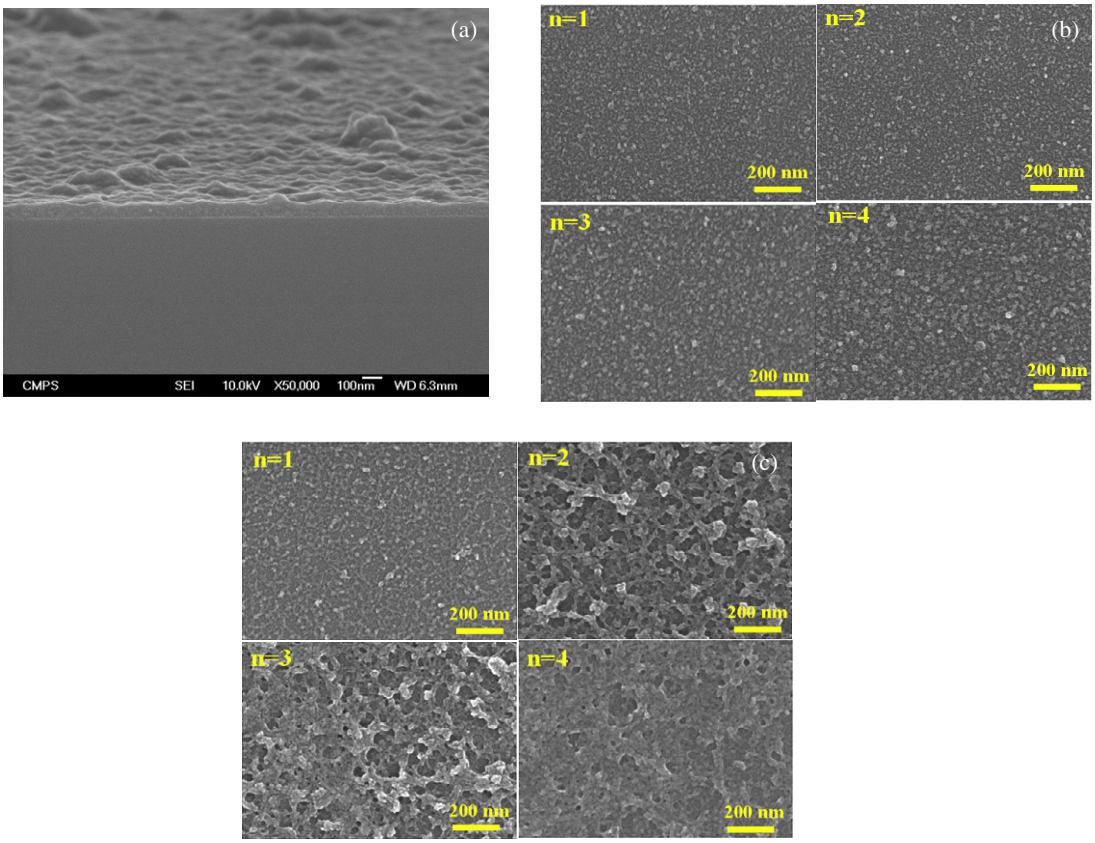

Figure 3. SEM images of (a) (PAH/dispersed CAT-Au_{NP})$_{10}$, (b) (PAH/CAT-Au_{NP} colloids)$_n$ and (c) (PSS/CAT-Au_{NP} network)$_n$ multilayers with increasing bilayer number (n). In this case, CAT-Au_{NP} colloids were encapsulated with PSS/PAH/PSS layers.

of specific binding between the amino acid groups and Au_{NP} places a limit on the growth of colloidal crystals. Here, we highlight the fact that the nanocomposite colloids in this system could be self-assembled through facile control of the solution pH without the aid of a colloidal substrate, such as polystyrene (PS), silica (SiO_2) or melamine formaldehyde (MF) colloids. The CAT-Au_{NP} colloidal crystals could be solubilized reversibly at pH $<$ 5 or pH $>$ 6 [6]. Furthermore, the consecutive LbL deposition of PSS/PAH/PSS onto the CAT-Au_{NP} composite colloids can encapsulate these colloids (i.e., zeta-potential after coating PSS on CAT-Au_{NP} ~ -40 mV and zeta-potential after the PAH coating $\sim +25$ mV) and increase the enzyme and nanoparticle loading per layer. For example, in the case of depositing (PSS/PAH/PSS)$_1$-encapsulated CAT-Au_{NP} colloids onto a PAH-coated QCM electrode at pH 5.2, the adsorbed amount of encapsulated colloids was approximately $\Delta m \approx 5\ \mu g\,cm^{-2}$ ($\Delta F \approx 411$ Hz). These CAT-Au_{NP} colloids inside the PE capsules could be reversibly dissolved by exposure to a solution at pH $>$ 6 or an acidic solution at pH $<$ 5. Another feature is that the increase in Au precursor concentration from 0.45 to 1.75 mM at a fixed amount of CAT causes the formation of gel composites with a network structure at pH 5.2, instead of colloidal composites (figure 2). Considering that the free amino and carboxylic acid groups of CAT unbound to Au_{NP} play an important role in forming the nanocomposite colloids, the relatively high concentration of the Au precursor decreases the amount of free amino and carboxylic acid groups of CAT significantly, as mentioned above. Therefore, the CAT-Au_{NP} composites have a network gel structure with a cationic surface at pH 5.2, which could not be encapsulated by PSS/PAH/PSS multilayers.

This structural transformation of CAT-Au_{NP} nanocomposite has a significant effect on the surface morphology of PE/CAT-Au_{NP} multilayers, as shown in the scanning electron microscopy (SEM) images of figure 3. That is, the surface morphology of (PAH/dispersed CAT-Au_{NP})$_{10}$ multilayers of about 85 nm thickness was uniform and smooth, while on the other hand (PAH/CAT-Au_{NP} colloids)$_4$ multilayers of about 92 nm thickness had a rugged and protuberant morphology reflecting the adsorption of CAT-Au_{NP} colloids. In the case of assembling the network-structured CAT-Au_{NP} layer with PSS at pH 5.2, these multilayer films had a fibrillary structure, compared to that of (PAH/dispersed CAT-Au_{NP})$_{10}$ or (PAH/CAT-Au_{NP} colloids)$_n$ multilayers (figure 3). The film thicknesses of (network CAT-Au_{NP}/PSS)$_n$ were increased from 128 nm to about 412 nm with increasing bilayer number (n) from 5 to 15. As a result, the thickness per layer was measured to be about 25.6 nm (see supporting information, figure S4 available at stacks.iop.org/Nano/21/375702/mmedia).

Here, the possibility that CAT-Au_{NP} nanocomposite multilayers can significantly increase their electrochemical reactivity cannot be excluded, because CAT-Au_{NP} with a pH-induced structural transformation can have an important effect

on the adsorbed amount of both the CAT showing the catalytic activity toward H_2O_2 and the Au_{NP} acting as an electrical relaying element between the CAT redox site and the electrode. The electrochemical behavior of $K_3Fe[CN]_6/C_6FeK_4N_6$ at the bare Au electrode, PAH/CAT, and three different types of PE/CAT-Au_{NP} multilayer-coated electrode surfaces in a pH 7.0 phosphate buffer solution (PBS) was investigated to determine the electronic communication behavior between the CAT-Au_{NP} and electrode. Generally, $K_3Fe[CN]_6/C_6FeK_4N_6$ undergoes a reversible electrochemical reaction on various electrodes, and is used widely as an electrochemical probe to examine the characteristics of functional films on electrode surfaces [31–33]. First, the adsorbed amount of all multilayer samples was fixed at about 9.63–9.90 $\mu g\ cm^{-2}$ through the control of the deposited layer number because the amounts adsorbed in these CAT-Au_{NP} nanocomposite multilayers increased significantly compared to those in $(PAH/CAT)_5$ multilayers (figure 4(a)). It should be considered that the total adsorbed amount of (PE/CAT-Au_{NP} network)$_5$ multilayers was about 5.7 times higher than $(PAH/CAT)_5$ multilayers at the same solution concentration. Based on these results, we investigated the ΔE_p of four different multilayers with controlled bilayer number (i.e., $(PAH/CAT)_5$, (PAH/dispersed CAT-$Au_{NP})_3$, (PAH/CAT-Au_{NP} colloids)$_1$ and (PSS/CAT-Au_{NP} network)$_1$ multilayers). In this case, the corresponding total adsorbed amount of CAT, dispersed CAT-Au_{NP}, and CAT-Au_{NP} network layers was about 9.63, 9.61, and 9.90 $\mu g\ cm^{-2}$, respectively. Additionally, we calculated the total amount of CAT and Au_{NP} in the three different films using QCM and thermogravimetric analysis (TGA): 4.85 and 0 $\mu g\ cm^{-2}$ for $(PAH/CAT)_5$, 1.34 and 8.27 $\mu g\ cm^{-2}$ for (PAH/dispersed CAT-$Au_{NP})_3$ and 1.58 and 8.32 $\mu g\ cm^{-2}$ for (PSS/CAT-Au_{NP} network)$_1$ (see supporting information, figure S5 available at stacks.iop.org/Nano/21/375702/mmedia). It should be noted that although the adsorbed amount of CAT (about 0.97 $\mu g\ cm^{-2}$) per layer in the $(PAH/CAT)_5$ multilayers was higher than that (i.e., 0.45 $\mu g\ cm^{-2}$) per layer in (PAH/dispersed CAT-$Au_{NP})_3$, the loading amount of CAT (i.e., 1.58 $\mu g\ cm^{-2}$) in the PSS/CAT-Au_{NP} network films was significantly increased. On the other hand, we did not calculate the adsorbed amount of CAT and Au_{NP} in the (PAH/CAT-Au_{NP} colloids)$_1$ exactly because CAT-Au_{NP} colloids were coated with PSS/PAH/PSS multilayers. In this case, the potential differences (ΔE_p) between the oxidation and reduction peak potential of $K_3Fe[CN]_6/C_6FeK_4N_6$ at the $(PAH/CAT)_5$, (PAH/dispersed CAT-$Au_{NP})_3$, (PAH/CAT-Au_{NP} colloids)$_1$ and (PSS/CAT-Au_{NP} network)$_1$ multilayer-coated ITO electrode were 520, 480, 450 and 425 mV at 50 mV s^{-1}, respectively (figure 4(b)). It was also observed that the respective ΔE_p values for the four different multilayers have standard deviations below 6% through variation tests from sample to sample. For example, the ΔE_p value deviations of $(PAH/CAT)_5$ and (PSS/CAT-Au_{NP} network)$_1$ nanocomposite using variation tests from sample to sample were ±30 and ±25 mV for (PSS/CAT-AuNP network)$_1$ films, respectively (see supporting information, figure S6 available at stacks.iop.org/Nano/21/375702/mmedia).

Considering that a smaller ΔE_p indicates a greater electron communication between $K_3Fe[CN]_6/C_6FeK_4N_6$ and the electrode, this phenomena reveals that the CAT-Au_{NP} nanocomposite, allowing structural transformation for the high loading of Au_{NP} as well as CAT, can significantly improve the electron transfer between $K_3Fe[CN]_6/C_6FeK_4N_6$ and the electrode in comparison to the PE/CAT multilayers without Au_{NP}. Furthermore, with increasing bilayer number (n) of (PSS/CAT-AuNP network)$_n$ multilayers from 1 to 7, the redox current of the multilayers was slightly increased. In particular, the redox peak separation of the multilayers was measured to be about 425 mV for 1 bilayers, 485 mV for 3 bilayers, 561 mV for 5 bilayers and 690 mV for 7 bilayers, respectively (see supporting information, figure S7 available at stacks.iop.org/Nano/21/375702/mmedia). These results imply that the increase of total film thickness restricts the effective electron transfer between $K_3Fe[CN]_6/C_6FeK_4N_6$ and the electrode. Although the increase of Au_{NP} amount within the nanocomposites has a significant effect on the enhancement of the electron transfer efficiency, we cannot exclude the possibility that the effective electron transfer may also be influenced by the porous structure of the (PAH/CAT-Au_{NP} colloids)$_1$ and the

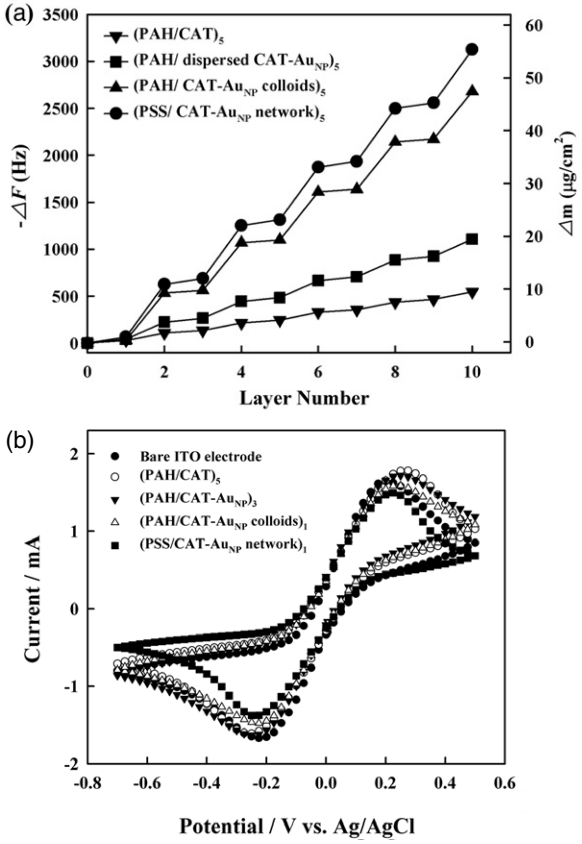

Figure 4. (a) Frequency and mass changes in the PAH/CAT and PAH/CAT-Au_{NP} multilayers with increasing layer number. These CAT-Au_{NP} deposited in aqueous solution have three different forms with a well-dispersed form, and good crystallization and network structure. (b) Cyclic voltammograms of 10 mM $K_3Fe[CN]_6/C_6FeK_4N_6$ in pH 7.0 PBS at a bare ITO electrode, $(PAH/CAT)_5$, (PAH/dispersed CAT-$Au_{NP})_5$, (PAH/CAT-Au_{NP} colloids)$_5$, (PSS/CAT-Au_{NP} network)$_5$ multilayer-coated electrodes.

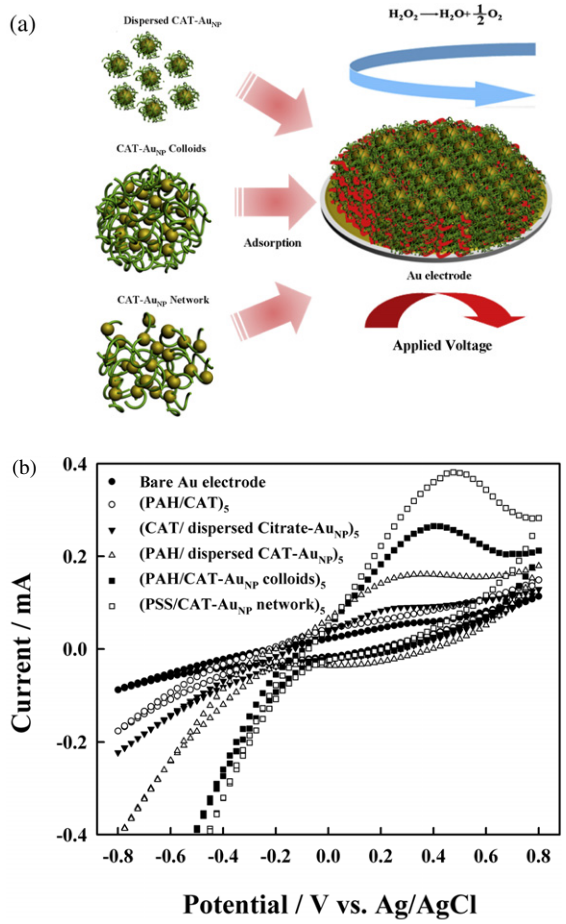

Figure 5. (a) Schematic for CAT-Au$_{NP}$-based electrochemical sensors showing the H_2O_2 decomposition. (b) Cyclic voltammograms of a bare Au electrode, (PAH/CAT)$_5$, (CAT/citrate-Au$_{NP}$)$_5$, (PAH/CAT-Au$_{NP}$)$_5$, (PAH/CAT-Au$_{NP}$ colloids)$_5$, and (PSS/CAT-Au$_{NP}$ network)$_5$ multilayer-modified electrodes in PBS containing 21 mM H_2O_2 at pH 7 with a scan rate of 50 mV s^{-1}. CAT-Au$_{NP}$ with a colloidal structure was encapsulated with PSS/PAH/PSS.

(PSS/CAT-Au$_{NP}$ network)$_1$ multilayers, as shown in the SEM images of figures 3(b) and (c). This hypothesis was supported by the fact that the ΔE_p value for (PAH/dispersed CAT-Au$_{NP}$)$_3$ was higher than that for (PAH/CAT-Au$_{NP}$ network)$_1$ films although the total amount of Au$_{NP}$ within two different nanocomposite films was almost the same. Additionally, an increase of inserted bilayers within the nanocomposite multilayers (i.e. (PAH/CAT)$_5$, (PAH/dispersed CAT-Au$_{NP}$)$_3$ and (PAH/CAT-Au$_{NP}$ colloids coated with PSS/PAH/PSS)$_1$) can partly contribute to the decrease of electron transfer efficiency by the gradual blocking of the electrode, inducing the Donnan exclusion effect. It was reported by Chirea *et al* that anionic electroactive species such as $[Fe(CN)_6]^{3-}$ have difficulty in infiltrating the multilayers with the outermost anionic layers due to electrostatic repulsion (or the Donnan exclusion effect) [34]. As a result, it is reasonable to conclude that the improved electron communication shown in CAT-Au$_{NP}$ nanocomposite films is caused by multiple effects such as the porous structure and gradual blocking of electrodes as well as the loading of metal nanoparticles.

Based on these results, hybrid electrochemical sensors composed of CAT-Au$_{NP}$ can be designed, as shown in figure 5(a). It was envisioned that the (PE/CAT-Au$_{NP}$) multilayers could show excellent electrocatalytic behavior toward H_2O_2 because CAT is an efficient catalyst for H_2O_2. In particular, the electrode modified with (PE/CAT-Au$_{NP}$ network)$_5$ multilayers of about 120 nm thickness showed the strongest oxidation peak potential at 0.5 V with a greater increase in peak current compared to those of about 28 nm-thick (PAH/CAT)$_5$, 42 nm-thick (PE/dispersed CAT-Au$_{NP}$)$_5$ and 110 nm-thick (PE/CAT-Au$_{NP}$ colloids)$_5$ multilayer-modified electrodes, suggesting that the network-structured CAT-Au$_{NP}$ have a highly catalytic activity toward H_2O_2 (figure 5(b)). The peak current at a (PE/CAT-Au$_{NP}$ network)$_5$-modified electrode linearly increases with increasing concentration of H_2O_2 from 5 to 21 mM (see supporting information, figure S8 available at stacks.iop.org/Nano/21/375702/mmedia). Therefore, the increased catalytic behavior of CAT-Au$_{NP}$ multilayers when transforming from a dispersed to a network structure is caused by the enhanced electron transfer as well as the increase in adsorbed amount of electrochemically active components. As mentioned above, the rugged and fibrillary structure of PE/CAT-Au$_{NP}$ colloids and PE/CAT-Au$_{NP}$ network multilayers has an increased surface area, and resultantly can induce enhancement of the direct contact area between the probe molecules and the CAT as well as the effective electron transfer. Therefore, this structural morphology may assist in the increase of electrochemical sensitivity. It should also be noted that multilayer sensors based on CAT-Au$_{NP}$ (particularly, CAT-Au$_{NP}$ network) are superior to those using (positively charged CAT/anionic citrate ion-stabilized Au$_{NP}$)$_n$ multilayers in view of the electrochemical sensitivity due mainly to the higher loading of CAT. That is, the adsorbed amount of positively charged CAT was measured to be about 0.50 μg cm^{-2} per layer onto the anionic citrate-Au$_{NP}$ layer. This amount was relatively low in comparison with that of CAT, of about 1.58 μg cm^{-2} per layer in the amount of CAT-Au$_{NP}$ network layer. Considering that CAT has catalytic activity toward H_2O_2, as mentioned above, it is reasonable to assume that the relatively low electrochemical sensitivity of (CAT pH 3/citrate-Au$_{NP}$ pH 3) multilayers shown in figure 5(b) would be caused by the low adsorbed amount of CAT, although the inserted citrate-Au$_{NP}$ may play a role in efficient electrical communication between the enzymes and electrode. Another disadvantage of (PE/CAT)$_n$ multilayers is that CAT has pH-dependent electrostatic properties and resultantly the multilayer assembly based on cationic CAT and anionic Au$_{NP}$ is only possible in a narrow pH range. More specifically, in the case of constructing the multilayers from the positively charged CAT at pH 3 and the citrate ion-stabilized Au$_{NP}$ (citrate-Au$_{NP}$) at pH 9, the stable and robust assembly of multilayers is not secure due to the charge reversal of CAT in the citrate-Au$_{NP}$ solution. This phenomenon indicates that the solution pH of citrate-Au$_{NP}$ should be controlled below the $pI \sim 5.6$ of CAT. As a result, our results suggest that the approach based on CAT-Au$_{NP}$ can easily control the sensitivity of sensors through facile electron transfer as well as a multilayer design in a broad pH range. In addition, the redox protein-stabilized Au$_{NP}$ has

important advantages in increasing the proteins and/or metal nanoparticle loading through pH-induced structural changes.

4. Conclusions

We have demonstrated that redox protein-encapsulated metal nanoparticles can have pH-dependent electrostatic properties and induce structural transformations with a high loading of CAT. At pH 5.2, the dispersed CAT-Au_{NP} were agglomerated into colloidal particles with a diameter size of about 50 nm or network-structured composites according to the initial concentration of gold precursor. Furthermore, nanocomposite multilayers (particularly, (PAH/CAT-Au_{NP} network)$_n$ multilayers) based on these hybrid nanoparticles show higher electrochemical activity than those based on conventional multilayered sensors due to the relatively high loading of CAT and the improved electron efficiency. This approach is expected to be beneficial to a variety of biocatalytic applications.

Acknowledgments

This work was supported by a KOSEF grant funded by the Korean government (MEST) (2008-0058617), and ERC Program of KOSEF grant funded by the Korean government (MEST) (R11-2005-048-00000-0). In addition, this work was supported by the Korea Research Foundation Grant funded by the Korean Government (KRF-2008-D00264, 2009-0085070).

References

[1] Marken F and McKenzie K J 2003 *Langmuir* **19** 4327
[2] Liu H, Rusling J F and Hu N 2004 *Langmuir* **20** 10700
[3] Shen L and Hu N 2005 *Biomacromolecules* **6** 1475
[4] Lvov Y and Caruso F 2001 *Anal. Chem.* **73** 4212
[5] Jin W, Shi X and Caruso F 2001 *J. Am. Chem. Soc.* **123** 8121
[6] Caruso F, Trau D, Möhwald H and Renneberg R 2000 *Langmuir* **16** 1485
[7] Nordgre N, Eklof J, Zhou Q, Brumer H III and Rutland M W 2008 *Biomacromolecules* **9** 942
[8] Cui X, Zhao Q, Sun Z and Jiang Z 2007 *Nanotechnology* **18** 215701
[9] Xiao Y, Patolsky F, Katz E, Hanifeld J F and Willner I 2003 *Science* **299** 1877
[10] Scott D, Toney M and Muzikar 2003 *J. Am. Chem. Soc.* **130** 865
[11] Sigel R K O and Pyle A M 2007 *Chem. Rev.* **107** 97
[12] Brown K R, Fox A P M and Natan M J 1996 *J. Am. Chem. Soc.* **118** 1154
[13] Xiao Y, Ju H and Chen H 2000 *Anal. Biochem.* **278** 22
[14] Gu H, Yu A and Chen H 2001 *J. Electroanal. Chem.* **516** 119
[15] Zhang J and Oyama M 2005 *J. Electroanal. Chem.* **577** 273
[16] Park J, Kim I, Shin H, Lee M J, Kim Y S, Bang J, Caruso F and Cho J 2008 *Adv. Mater.* **20** 1843
[17] Zayats M, Katz E, Baron R and Willner I 2005 *J. Am. Chem. Soc.* **127** 12400
[18] Decher G 1997 *Science* **277** 1232
[19] Caruso F, Caruso R A and Möhwald H 1998 *Science* **282** 1111
[20] Yu A and Caruso F 2003 *Anal. Chem.* **75** 3031
[21] Ghan R, Shutava T, Patel A, John V T and Lvov Y 2004 *Macromolecules* **37** 4519
[22] Zhang H, Lu H and Hu N 2006 *J. Phys. Chem.* B **110** 2171
[23] Cho J, Hong J, Char K and Caruso F 2006 *J. Am. Chem. Soc.* **128** 9935
[24] Hong J, Bae W, Oh S, Lee H, Char F and Caruso F 2007 *Adv. Mater.* **19** 4364
[25] Lee J-S, Cho J, Lee C, Kim I, Park J, Kim Y, Shin H, Lee J and Caruso F 2007 *Nature Nanotechnol.* **2** 790
[26] Lee B, Kim Y, Lee S, Kim Y S, Wang D and Cho J 2010 *Angew. Chem. Int. Edn* **49** 359
[27] Su X, Kim B-S, Kim S R, Hammond P T and Irvine D J 2009 *ACS Nano* **11** 3719
[28] Sheptovitsky Y G and Brudvig G W 1996 *Biochemistry* **35** 16255
[29] Hara I, Ichise N, Kojima K, Kondo H, Ohgiya S, Matsuyama H and Yumoto I 2007 *Biochemistry* **46** 11
[30] Buttry D 1991 Applications of the QCM to electrochemistry *A Series of Advances in Electroanalytical Chemistry* (New York: Dekker)
[31] Harris J J and Bruening M L 2000 *Langmuir* **16** 2006
[32] Pardo-Yissar V, Katz E, Lioubashevski O and Willner I 2001 *Langmuir* **17** 1110
[33] Yu A, Liang Z, Cho J and Caruso F 2003 *Nano Lett.* **3** 1203
[34] Chirea M, Garcia-Morales V, Manzanares J A, Pereira C, Gulaboski R and Silva F J 2005 *Phys. Chem.* B **109** 21808